**RESEARCH ARTICLE**

**ISSN: 2321-7758**

# X-RAY SPECTROSCOPY OF PLASMAS OUTSIDE THERMODYNAMIC EQUILIBRIUM

## Dr. MOUSTFA M.H ESHTEWI

Sirt University, Libya

**ABSTRACT**

The current study explores the X-ray emission of niobium, tantalum and tungsten plasmas, under conditions outside local thermodynamic equilibrium (of the order of 1.5keV in temperature, and $10^{20}$ cm$^{-3}$ in density electronic). It was measured the X-ray spectrum in the 2.4-2.9 keV range using a tapered crystal spectrometer. It was also implemented hydrodynamic diagnostics (Thomson diffusion and clean emission resolved in time) in order to properly characterize the plasma studied. A study is underway to compare the measurements with the simulations. Here the comparison was made on the hydrodynamic measurements to the MULTI code to adjust certain unknown experimental parameters and determine the evolution of the plasma, then use these results in the spectral calculations carried out using the FLYCHK code.

Keywords: Plasma, Thermodynamic equilibrium, atomic physics, X-ray spectroscopy

## 1. INTRODUCTION

The subject of this paper is a part of the general context of the study radiative properties of hot plasmas. The "plasma" state constitutes the fourth state of matter, following in the temperature scale the so-called "classic" states: solid, liquid and gas. It is a dilute state made up of charged particles - electrons and positive ions - in proportion such that the medium is generally neutral. Plasmas represent a significant percentage of our environment. Present mainly in the Universe, they are found in astrophysical objects such as stars, or even planetary atmospheres to cite a few examples.

Generated by and heated by laser radiation, hot plasmas emit in a wide range of the electromagnetic spectrum: radio-electric radiation with X-rays. The radiative emission of laboratory plasmas constitutes a true indicator of their density, temperature and their state of ionization. Thus, the study of these plasmas involves many fields such as atomic physics, statistical physics, hydrodynamic equations and finally the equations of radiative transfer.

The study of plasmas outside of local thermodynamic equilibrium is very general since they can be astrophysical plasmas, X laser plasmas, or many laboratory plasmas. These plasmas are difficult to characterize and the emission calculations are complex under these conditions. L and M layer emission spectroscopy for plasmas outside local thermodynamic equilibrium is still little studied: the emission depends on the temporal evolution of the plasma, the calculations are complex and experimental measurements are necessary to validate them. These measurements must aim to characterize the emitting plasma, from a hydrodynamic point of view, in order to constrain the codes of atomic physics. Our team has already carried out several experimental campaigns of this type, on other elements (Xe, Kr, Br) [1–3], during which the experimental setup was gradually improved and enriched with new diagnoses.

The purpose of the experiment presented here was to study the L-layer emission of niobium plasmas, and the M-layer emission of tantalum and tungsten plasmas. The spectroscopic properties of tungsten, used in the walls of tokomaks, are important for fusion plasmas by magnetic confinement. This study carried out spectroscopic and hydrodynamic measurements and compared

these results with medullisations using codes MULTI (hydrodynamics) [4] and FLYCHK (atomic physics) [5].

## 2. CONDITIONS OUTSIDE LOCAL THERMODYNAMIC BALANCE

Plasmas are rarely in thermodynamic equilibrium (a single temperature for electrons, ions and radiation, energy and ionization states distributed according to Boltzmann and SahaBoltzmann law, radiation according to Planck's law). However, when the number of collisions is large enough, that the temporal evolution of the system is not too fast and that the density and temperature gradients are not too strong, locally have thermalization of the system. The electrons and ions are then in local thermodynamic equilibrium (ETL). When this local equilibrium is not reached and speak of plasma outside local thermodynamic equilibrium (HETL). In this case, one must take into account the temporal evolution of the plasma and the electronic and ionic populations resulting from a radiative collisional equilibrium; the calculations become significantly more complex. The detailed atomic physics codes are capable of calculating the emission of a HETL plasma. However, when it is necessary to take into account the temporal evolution of the plasma to calculate the emission, simplified codes are used so that the calculation time is not prohibitive and so that they can be coupled to hydrodynamic codes. It may happen that the calculations are no longer sufficiently precise to properly describe the experimental results measured. The codes calculating the HETL emission of a plasma use many hydrodynamic parameters (temperature, density...), and the results of the calculations vary greatly with these parameters. To validate the codes, it is therefore necessary to constrain these hydrodynamic parameters. This requires carrying out experiments measuring simultaneously and independently the hydrodynamic evolution of the plasma and its emission.

## 3. REALIZATION OF THE EXPERIENCE

3.1. Experimental setup and targets used The plasma was created and heated by two laser beams forming an angle of 10˚, of wavelength 532 nm, synchronous, with a duration of 1.5 ns, focused on 400 m in diameter at l using phase blades (HPP), for a total intensity of the order of 4 × 1014 W / cm². The studied plasmas of niobium, tungsten and tantalum, using two types of Solid targets: massive targets and so-called "dowry" targets. The massive targets were 5m thick metal sheets. The "dots" targets consisted of a stud of the material studied, 10 m thick and 400 m in diameter, deposited on a CH / Au / CH multilayer substrate. This type of target makes it possible to approach a one-dimensional expansion of the plasma studied [6,7] which improves the chances of correctly describing the hydrodynamic evolution of the plasma using a 1D code. The plasma thus created was observed at using multiple diagnostics. X-ray emission was recorded using a time-integrated spectrometer, observing the emission from plasma from the target surface up to + 300 m. The spectrometer consisted of a frustoconical crystal (a KAP crystal curved along a portion of a cone) and a photostimulable screen (imaging plate). He observed the energy range 2.4-2.9 keV, corresponding for niobium (Z = 41) to 3d-2p transitions (L layer), and for tantalum (Z = 73) and tungsten (Z = 74) at the 5f3d transitions (layer M). The raw image obtained depends on the surface defects of the crystal, as well as on wavelength variations in the reflectivity of the crystal and the transmission of the filters. It must therefore be corrected using a reference image, produced during a firing on a copper target whose emission is uniform in the energy field of interest. A spectral calibration was made using the observation of the lines of the K layer of chlorine, with a shot on PVDC (polyvinylidene chloride).

A first hydrodynamic diagnosis was the Thomson diffusion, the principle of which is summarized in the following paragraph. It was used a probe beam, wavelength 1064 nm, of the same length as the pump beams, but with a variable delay between 0.5 and 4.5 ns with respect to them. It was also varied the region of the probed plasma, from + 500 to + 1500 m from the target surface. The incidence of the probe beam was 45˚ from the direction of the plasma, in the plane of the heating beams. It was observed the scattering of the probe beam collected from above the target, and resolved spectrally and temporally thanks to two spectrometers associated with slit scanning cameras.

These hydrodynamic measurements were supplemented by a diagnosis of self-emission (self opticalpyrometry or SOP) resolved in space (1D) and in time. The formation of plasma by the heating beams induces a shock which propagates in the target. This shock generates an emission likely to escape from the target if it is transparent. In the case of the "dot" target, the plastic layer at the rear of the target being transparent, it was observed the clean emission during the whole crossing of the last layer. Visible field radiation was collected by a lens that imaged the rear of the target on a streak camera. It was thus possible to record the propagation of the shock resolved temporally: the duration of the measured emission corresponds to the crossing time of the last layer. Knowing its thickness, and knowing that the speed of the shock is constant in the layer, we can go back to the speed of propagation.

## 3.2. Principle of Thomson diffusion diagnosis

By observing the scattering of a probe beam by the charged particles of a plasma, the Thomson scattering allows us to go back to the hydrodynamic parameters of the latter. Depending on the characteristics of the laser, the plasma and the geometry of observation, the scattered spectrum translates the behavior either individual or collective of the particles. This spectrum depends on the temperatures and densities of the plasma which can thus determine.

It was measured collective scattering on electronic and ionic acoustic plasma waves. Let $k_{plasma}$ be the wave vector of the plasma wave on which the probe is scattered. In the case of scattering by ionic acoustic waves ("Thomson ionic"), the scattered satellites are shifted by the probe frequency in proportion to the acoustic speed $c_s$. By denoting Z the average plasma ionization, $T_e$ and $T_i$ the electronic and ionic temperatures, $m_i$ the mass of $\lambda_{De}$ an ion and Debye's length, this speed is given by equation (1).

$$c_s = \left[ \frac{ZT_e}{m_i \left( 1 + k_{plasma}^2 \lambda_{De}^2 \right)} + \frac{3T_i}{m_i} \right]^{1/2}. \qquad (1)$$

In the case of scattering by electronic plasma waves ("Thomson electronics"), the scattered satellites are

shifted by the probe frequency in proportion to the Bohm-Gross $\omega_{BG}$ frequency. By noting $n_e$ the electron density of the plasma $m_e$ and the mass of an electron, the frequency is given by equation (2).

$$\omega_{BG} = \left[ \frac{n_e e^2}{m_e \epsilon_0} \left( 1 + 3k_{plasma}^2 \lambda_{De}^2 \right) \right]^{1/2}. \qquad (2)$$

Our experience produces plasmas such as $k_{plasma} \lambda_{De}$ <1 and $T_i \ll T_e$. One thus obtains using the equations (1) and (2), a relation between the separation of the ionic satellites and the product $ZT_e$ on the one hand, and between the separation of the electronic satellites and $n_e$ the other hand.

Electronic satellites are therefore spread proportionally to $n_e^{1/2}$ e and ionic satellites proportionally to $(ZT_e)^{1/2}$. To this is generally added a Doppler shift due to duplasma expansion: the probe frequency perceived by the particles is shifted, then the frequency emitted by these same particles is shifted for the detector. The total $\lambda_{Doppler}$ shift, for a measurement along the axeperpendicular to the target at its center, is given by equation (3). We note $\lambda_{probe}$ the wavelength of the probe beam, and $v_{exp}$ the speed of expansion in the direction orthogonal to the target.

$$\Delta \lambda_{Doppler} = -\frac{\lambda_{probe}}{\sqrt{2}} \frac{v_{exp}}{c} \qquad (3)$$

As the ionic acoustic pulsation is much smaller than the electronic plasma pulsation, two spectrometers are used, one with very good resolution in a small range around the probe frequency, the other covering a much wider range. We observed the two ion satellites, but only one electronic satellite (the one shifted towards the blue), the spectral range of our detector not being sufficiently broad to observe the two electronic satellites. Figure 1 showsthe satellites observed, and a spectrum resolved in Thomson time. The use of slit-scanning cameras makes it possible to obtain measurements that are resolved in time. We have obtained good reproducibility of the measurements for a given time and position. By varying the delay of the probe beam and the region probed, we were able to extend our observations of the evolution of plasmas at different times and positions along the longitudinal axis.
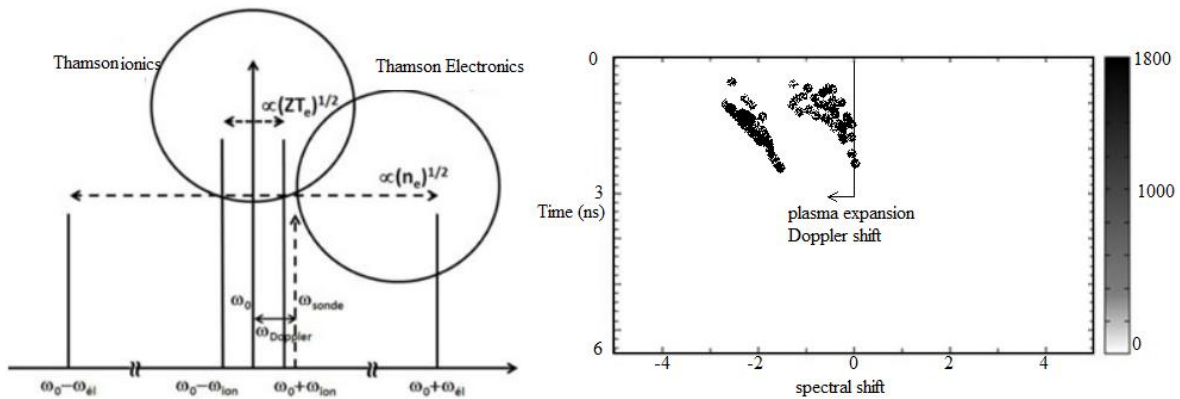
Figure 1: Left: diagram of Thomson ion and electronic scattering. Right: experimental spectrum resolved in Thomson ion diffusion time.

## 4. COMPARISON TO DIGITAL CODES

The hydrodynamic parameters of the plasma are measured by the Thomson diagnosis in the crown (sufficiently sparse for the probe beam to propagate) and by the diagnosis of SOPen rear face of the target. However, the spectra recorded come from denser and warmer regions, close to the surface of the target, and it is the evolution of the emissive region that matters for a code of atomic physics. It is therefore necessary to reconstruct the hydrodynamic evolution of this region in order to be able to model the spectra obtained.

The approach that we adopted was to use hydrodynamic simulations, using the MULTI code (1D calculations), and our objective being initially to reproduce the measurements of the hydrodynamic diagnostics in order to have confidence in our description of the evolution of the plasma, then deduce from these simulations the evolution of the region observed by the spectrometer.

### 4.1. Hydrodynamic modeling of plasma

The first step was to adjust the incident laser intensity on a dot-type target so that the simulation reproduced the delay measured using the SOP. For each SOP image, we were able to measure a delay and associate a laser intensity with it. Depending on the shots, the delays were 0.88 to 1.33 ns and the associated intensities between $5 \times 10^{13}$ W / cm$^2$ (1.33 ns) and $10^{14}$ W / cm$^2$ (0.88 ns). Figure 2 shows the imagery by the SOP for a shot on a dowry of niobium, and the simulation reproducing the measured delay (intensity on target of $5 \times 10^{13}$ W / cm$^2$). In the SOP image, time runs from top to bottom, the dot is spatially centered. We first observe the outlet of the shock outside the dowry and then, at dudot level, the emission due to the propagation of the shock in the plastic layer (around 2.5 to 4 ns). By knowing the thickness of this layer we can calculate the speed of propagation of the shock in the plastic. The simulation provides a compression map in the target over time. In this experiment the laser arrives from the left on the dot, and the shock generated crosses the different layers of the target (located above the map). The successive slopes correspond to the different impact speeds. We can therefore calculate the crossing time of the last layer, to compare with the SOP measurement.
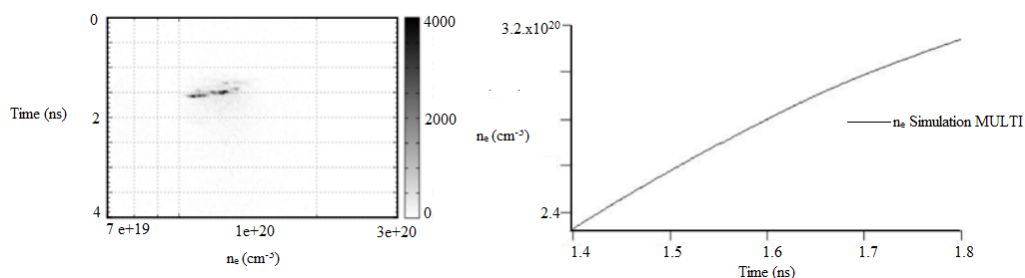


Figure 2. Comparison of the electron density deduced from the Thomson electron scattering, 500 m from the front face of the target, 1.5 ns after the start of the heating beams, with the results of the MULTI simulation

Dr. MOUSTFA M.H ESHTEWI

![Impact Factor 5.8701 (ICI)]

International Journal of Engineering Research-Online
*A Peer Reviewed International Journal*
Articles available online http://www.ijoer.in; editorijoer@gmail.com

**Vol.6., Issue.6, 2018**
**Oct-Dec.,**

(laser intensity of $5\times10^{13}$ W / cm$^2$). The experimental image is resolved in time vertically and the spectral axis has been converted to electronic density.
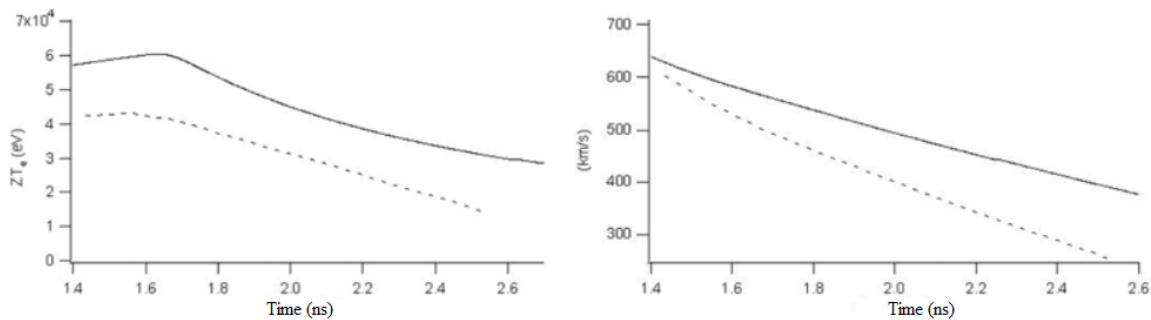


Figure 3. Comparison of the ZT$_e$ product and the expansion speed deduced from the Thomson ion scattering, at + 500 m from the target, with the results of the MULTI simulation (laser intensity of $5\times10^{13}$W / cm$^2$).

Secondly, we compared the Thomson diffusion measurements to the simulation results. Figures 2 and 3 show the Thomson scattering measurements on the same dot of niobium, 500 m from the front face of the target, with a delay of 1.5 ns compared to the start of the heating beams, compared to the results of the simulation. MULTI for a laser intensity of $5\times10^{13}$/cm$^2$ (reproducing the SOP measurement). Despite a simulation limited to one dimension, we get a fairly good agreement. The temporal evolutions are qualitatively well reproduced, with however an overestimated ZT$_e$. The expansion rate, which was very good at first, is also overestimated thereafter, which is consistent with an overestimation of T$_e$. The calculated electronic density is also of the order of magnitude.

### 4.2. First spectral analyzes

We used the results of the hydrodynamic simulations in the spectrometer observation area to calculate a spectrum. The conditions obtained for the plasma zone which is observed the emission are of the order of 1.5 keV and 1020 cm −3. First calculations were made using the FLYCHK code, taking into account a finite detailed plasma, divided into 399 uniform zones corresponding to the MULTI simulation grid, and assuming that all the radiation escapes. The results are still being analyzed, we will therefore present here only these first calculations. Figure 4 shows a spectrum calculated with the FLYCHK code from the MULTI simulation at $5\times10^{13}$W /cm$^2$ and the spectrum recorded during of a shot on a dowry of niobium, with the states of ionization corresponding to the lines. The calculated spectrum is integrated in time and comes from the most

emissive area of the region observed. We observe that the experimental spectrum has many structures which are not reproduced by the calculations, this is probably due to the relatively small number of transitions taken into account in the code (which uses the Super Transition Array formalism). In addition, the emission measured seems to come from a hotter and ionized plasma than the simulations predict. It will therefore be necessary to go further in the simulation, in particular by considering the real size of the plasma, the effects of opacity and the interactions between the different zones.
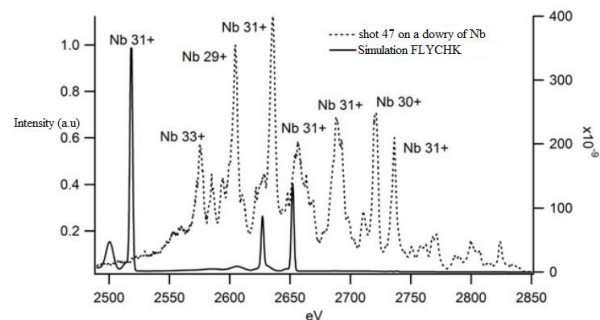


Figure 4. Comparison between the experimental spectrums of a dot Niobium (shot 47) and a spectrum simulated with the code FLYCHK, using MULTI simulation with laser intensity of $5\times10^{13}$W/cm$^2$.

### 5. CONCLUSION

During this experience we were able to simultaneously obtain good quality measurements on our three diagnoses. Hydrodynamic simulations prove to be consistent with diffusion measurements Thomson and SOP, which indicate that they are a good tool for modelling the evolution of plasma. We

used these simulations to perform spectroscopic calculations using the FLYCHK code.

The first calculations, if they do not account for all the emission observed, show the importance of performing spectral measurements coupled with measurements allowing a good description of the plasma in order to test the codes. They will be continued in order to specify them, taking into account for example the opacity of the plasma and the entire area observed. The use of an atomic physics code which uses statistical methods [8,9], like TRANSPEC [10–12], can also be interesting, in order to take into account a greater number of transitions, in particular on heavy elements (tantalum tungsten). A time-resolved spectroscopy measurement (which would give a better idea of the conditions under which the dominant part of the spectrum is emitted) is planned for a future experiment in order to complete our study.

## References

[1]. Busquet, Michel. (1993). Radiation-dependent ionization model for laser-created plasmas. Physics of Fluids B. 5. 10.1063/1.860586.

[2]. Koningsberger, D. C. & Prins, R. X-Ray Absorption: Principles, Applications, Techniques of EXAFS, SEXAFS and XANES. (J. Wiley & Sons, New York, 1988)

[3]. Cavalleri, A. et al. Band-selective measurements of electron dynamics in VO2 using femtosecond near-edge X-ray absorption. Phys. Rev. Lett. 95, 067405 (2005)

[4]. Lifschitz, A. et al. Particle-in-cell modelling of laser–plasma interaction using Fourier decomposition. J. Comput. Phys. 228, 1803 (2009)

[5]. M. I. Boulos, P. Fauchais, and E. Pfender, Thermal Plasmas: Fundamentals and Applications (Plenum Press, New York, 1994),

[6]. A. B. Murphy and D. Uhrlandt, Plasma Sources Sci. Technol. 27, 063001 (2018).

[7]. P. G. Burkhalter, M.J. Herbst, D. Duston, J. Gardner, M. Emery, R.R Whitlock, J. Grun, J.P.Apruzese, J. Davis, Phys. Fluids 26, 3650 (1983)

[8]. K. S. Novoselov, A. K. Geim, S. V. Morozov, D. Jiang, Y. Zhang, S. V. Dubonos, I. V. Grigorieva, and A. A. Firsov, Science 306, 666 (2004).

[9]. Dorchies, F. & Recoules, V. Non-equilibrium solid-to-plasma transition dynamics using XANES diagnostic. Phys. Rep. 657, 1 (2016).

[10]. A.-C. Bourgaux, S. Bastiani-Ceccotti,et al.,, Spectroscopie X de couches L et M de plasmas hors équilibre thermodynamique local de niobium, tantale et tungstène (French),UVX 2012, 01006 (2013)

[11]. Dorchies, F. et al. Unraveling the solid–liquid–vapor phase transition dynamics at the atomic level with ultrafast X-ray absorption near-edge spectroscopy. Phys. Rev. Lett. 107.24, 245006 (2011).

[12]. Rousse, A. et al. Production of a keV X-ray beam from synchrotron radiation in relativistic laser-plasma interaction. Phys. Rev. Lett. 93, 135005 (2004).

Dr. MOUSTFA M.H ESHTEWI